


Article

High-Strength Welding of Silica Glass Using Double-Pulse Femtosecond Laser under Non-Optical Contact Conditions

Zheng Gao ¹, Jiahua He ², Xianshi Jia ^{1,*} , Zhaoxi Yi ¹, Cheng Li ¹, Shifu Zhang ¹, Cong Wang ¹ and Ji'an Duan ¹

¹ State Key Laboratory of Precision Manufacturing for Extreme Service Performance, College of Mechanical and Electrical Engineering, Central South University, Changsha 410083, China; 233712195@csu.edu.cn (Z.G.); 193701001@csu.edu.cn (Z.Y.); licheng_csu@csu.edu.cn (C.L.); zhangshifu_csu@csu.edu.cn (S.Z.); wangcong@csu.edu.cn (C.W.); duanjian@csu.edu.cn (J.D.)

² Shanghai Aerospace Control Technology Institute, Shanghai 201109, China; zhipingchai@hust.edu.cn

* Correspondence: 221026@csu.edu.cn

Abstract: Ultrafast laser welding technology for transparent materials has developed rapidly in recent years; however, high-strength non-optical contact transparent material welding has been a challenge. This work presents a welding method for silica glass using a double-pulse femtosecond (fs) laser and optimizes the laser processing parameters to enhance the welding performance. The welding characteristics of silica glass are analyzed under different time delays by controlling the pulse delay of double pulses. In addition to comprehensively study the influence of various experimental conditions on double-pulse fs laser welding, multi-level tests are designed for five factors, including average laser power, pulse delay, scanning interval, scanning speed, and repetition rate. Finally, by optimizing the parameters, a welding strength of 57.15 MPa is achieved at an average power of 3500 mW, repetition rate of 615 kHz, pulse delay of 66.7 ps, scanning interval of 10 μm , and scanning speed of 1000 $\mu\text{m/s}$. This work introduces a new approach to glass welding and presents optimal parameters for achieving higher welding strength, which can be widely used in aerospace, microelectronic packaging, microfluidics, and other fields.

Keywords: femtosecond laser; laser welding; optical contact; glass



Citation: Gao, Z.; He, J.; Jia, X.; Yi, Z.; Li, C.; Zhang, S.; Wang, C.; Duan, J. High-Strength Welding of Silica Glass Using Double-Pulse Femtosecond Laser under Non-Optical Contact Conditions. *Photonics* **2024**, *11*, 945. <https://doi.org/10.3390/photonics11100945>

Received: 6 September 2024

Revised: 27 September 2024

Accepted: 30 September 2024

Published: 8 October 2024



Copyright: © 2024 by the authors. Licensee MDPI, Basel, Switzerland. This article is an open access article distributed under the terms and conditions of the Creative Commons Attribution (CC BY) license (<https://creativecommons.org/licenses/by/4.0/>).

1. Introductions

Glass has good optical properties and physical stability, making it widely used in numerous industries such as construction [1], communication [2–4], the military industry [5,6], biomedicine [7–9], and other fields. In many applications, connections between two or more pieces of glass are often required. Various interface bonding methods for glass have been developed, including adhesive bonding [10], tin welding [11], direct bonding [12], fusion welding [13], anode bonding [14], and laser welding [15]. Among these methods, conventional laser welding uses continuous wave or long-pulsed lasers, with CO₂ lasers being commonly used [15]. For non-transparent materials, laser energy absorption is linear. The laser energy is absorbed by the non-transparent material surface through linear absorption, and then the two processed samples can be connected after the material is melted and solidified [16–19]. Glass is transparent, making it challenging for CO₂ laser energy to be absorbed, which is essential for welding. To facilitate welding with continuous or long-pulsed lasers, an intermediate absorption layer is required between the glass pieces to capture and transfer the laser energy [19]. In addition, with the trend toward the miniaturization of devices, some sophisticated instruments require high welding strength and precision. The machining accuracy of continuous or long-pulsed lasers is limited and unable to meet the latest demand.

Twenty years ago, the solution to this dilemma was proposed through glass welding using ultrafast lasers. Ultrafast lasers are capable of achieving high processing quality and efficiency [20–22], making it with wide application in material removal [23–25], cutting [26],

welding [27,28], and other processes. Ultrafast laser welding technology presents several advantages over traditional welding methods. The ultrashort pulse durations, ranging from femtoseconds to picoseconds, facilitate nonlinear absorption mechanisms within the material, enabling localized energy deposition without significantly heating the surrounding areas [29]. This capability results in minimal heat-affected zones and reduced thermal distortion, thereby preserving the integrity of the glass's material properties. Furthermore, ultrafast lasers can achieve high peak powers, which induce a "cold welding" effect, allowing materials to be joined without substantial melting—a feature particularly advantageous for thermosensitive materials like glass. The welding mechanism involves the interaction of intense laser pulses with the glass, leading to multiphoton ionization and the formation of a plasma channel. This plasma channel efficiently absorbs laser energy, creating a localized temperature rise that facilitates the melting and joining of the glass without the necessity for an intermediate absorption layer. The excited material's thermal response process is extremely short, and the heat-affected zone generated by the interaction between laser and material can be controlled in the scale of micrometers (μm) or even nanometers (nm), which overcomes the limitations of glass welding by continuous or long-pulsed laser. For example, Tamaki et al. published a work on femtosecond laser glass welding, which could achieve laser glass welding without adding an intermediate medium. In their research, a low single pulse energy of 1 μJ was used for welding, while the average power was 1 mW. However, the processing speed was only 5 $\mu\text{m}/\text{s}$, and the connection strength was not given quantitatively [30]. The following year, the same research group proposed the method of welding different types of glasses with a femtosecond laser, and the parameters were the same as before. The welding between borosilicate glass and fused silica was achieved in this experiment, which is difficult to achieve using conventional laser welding methods, and the welding strength reached 15.3 MPa [31]. Then, Watanabe et al. conducted a systematic study of femtosecond laser welding strength under different laser parameters for optimizing glass substrate connection at a low repetition rate, and they obtained a welding strength of 15.4 MPa by optimizing the welding strategy [32]. Richter et al. reported the welding of fused silica with ultrafast laser pulses at high repetition rates. By optimizing the welding parameters, the welding strength could reach 75% of the damage threshold of the material itself [33]. Hélie et al. used femtosecond laser welding technology to realize the direct connection of optical materials. This connection technology could achieve the connection of two materials with a large difference in thermal expansion coefficient, and the welded samples had high thermal shock resistance [34]. Kim et al. proposed a laser-machined glass microfluidic device manufacturing process. Microfluidic channels were carved on a glass substrate by femtosecond laser-assisted selective etching. The glass interface near the microfluidic channel was partially melted by direct welding, resulting in higher welding strength than the conventional bonding method [35]. Yu et al. used a 75 W green femtosecond laser equipped with a 255 mm long focal scanning galvanometer to achieve non-optical contact and high-speed welding of display screen glasses. The welding speed could reach 6 m/min, and the shear strength could reach 20 MPa [36]. Zhang et al. studied the transient temperature field and stress field when the small glass pieces were welded to the solder glass [37]. The effects of laser average power and welding speed on temperature and stress field during welding were analyzed. They found that the center temperature of the heat source increased with the increase in the average laser power and the decrease in the welding speed.

Although excellent welding strength has been achieved in previous studies, in most cases, optical contact between the surfaces of the two glasses was required. This means that the surfaces facing each other must have an extremely high degree of finish and flatness, which is difficult to achieve under general processing conditions and increases the manufacturing cost. Additionally, the method of welding glass directly in a non-optical contact condition with an ultrafast laser has reached a bottleneck in achieving further strengthened connections. Recently, researchers have proposed a new method of double-pulse femtosecond laser welding. Sugioka et al. used an ultrafast laser double pulse

sequence for direct welding of transparent materials such as glass, where the time-domain shaping technology of the ultrafast laser was used to precisely adjust the pulse delay of the double pulse sequence. By optimizing the welding parameters, the strength of the double-pulse welding was increased by 22% relative to single-pulse welding [38]. However, the parameters studied were not comprehensive and not fully compared, and the improvement in welding strength was not very significant.

Therefore, it is more practical to study how to improve the welding strength of silica glass in a simpler method under non-optical contact conditions. To address these issues, we propose a jig-free method to weld silica glass by femtosecond laser double-pulse under a non-optical contact condition. By adjusting the optical path of two pulsed laser beams, the time difference in reaching the sample to be processed can be controlled, allowing for double-pulse processing. This method has conducted a multi-level analysis of five factors and further explored the influence of different experimental conditions on welding. By optimizing the parameters, the welding strength obtained by this method is higher than before. Temperature resistance tests have also been carried out in combination with the extreme environments that may occur in actual applications.

2. Materials and Methods

The experimental device is shown in Figure 1, and Figure 1a is the schematic diagram of the double-pulse processing system. The femtosecond laser (Pharos from Light Conversion, Vilnius, Lithuania) emits laser through a shutter (SH) to a beam splitter (BS). The beam splitter divides it into two laser beams, which are, respectively, directed at the mirrors M1 and M2. These two mirrors are fixed on a one-dimensional moving platform. With the reflection of M1 and M2, the two laser beams are synthesized into one laser beam and directed to the mirror M3. Finally, the laser beam is focused on the silica glass sample (S) through the objective lens (OL). The silica glass is placed on a three-dimensional motion platform (P) controlled by the computer. Additionally, a CCD camera, lens (L), and objective lens (OL) constitute the microscopic imaging system for real-time detection and auxiliary control of double pulse. The light (Lt) and semi-reflective mirror (M4) provide illumination. The CCD camera on the side is used to adjust the position of the focus. For the experiment, a circular silica glass with a diameter of 10 mm and a thickness of 2 mm was selected for welding. Prior to processing, anhydrous ethanol and deionized water were, respectively, used for ultrasonic cleaning, a process lasting for 30 min. As shown in Figure 1c, the interval between layers (D) is 50 μm , the number of layers (N) is 7, and the scan height (Z) is 300 μm , enabling the silica glass to be melted in the entire processing area without requiring sufficient smoothness and flatness. The scan line length (l) is 1000 μm , and the scan line interval (d) is a variable. Figure 1b shows the schematic diagram of welding silica glass. The silica glass was welded with an objective lens (magnification 10 \times , numerical aperture 0.25), and the welding area was adjusted at the interface of the two glasses. After the scanning was completed, a heat-affected zone of 1000 μm \times 1000 μm \times 300 μm was formed. To prevent the stepper motor from instability and excessive laser energy from damaging the focusing objective lens at high speed, the maximum processing speed was limited to 2 mm/s, the laser power was limited to 3500 mW, and the energy ratio of the two laser beams was fixed at 1:1. The welding strength was tested by a tensile tester (HP-500, HANDPI, Germany), the device has a measuring range of up to 5 N and the accuracy of the device is 95%.

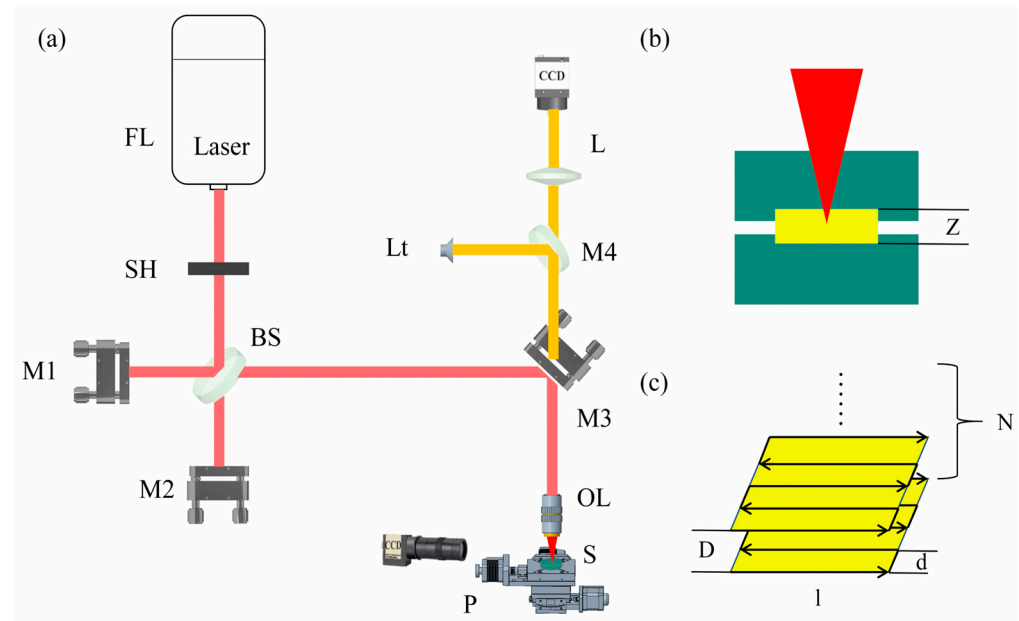


Figure 1. (a) Schematic diagram of double-pulse processing system. (b) Schematic diagram of welding silica glass. (c) Scan strategy diagram. FL, laser; SH, shutter; BS, beam splitter; M1, mirror; M2, mirror; M3, mirror; M4, mirror; L, lens; Lt, light; OL, objective lens; S, sample; P, three-dimensional motion platform.

3. Results and Discussion

3.1. Effect of Double-Pulse Delay on Silica Glass Welding Performance

To investigate the effect of pulse delay on welding, the characteristics of femtosecond laser glass welding under different pulse delays were studied. The delay time between the two pulses was regulated by adjusting the one-dimensional motion platform. The displacement of the one-dimensional platform and the pulse delay have a corresponding relationship given by

$$\tau = 0.5c / \Delta x \quad (1)$$

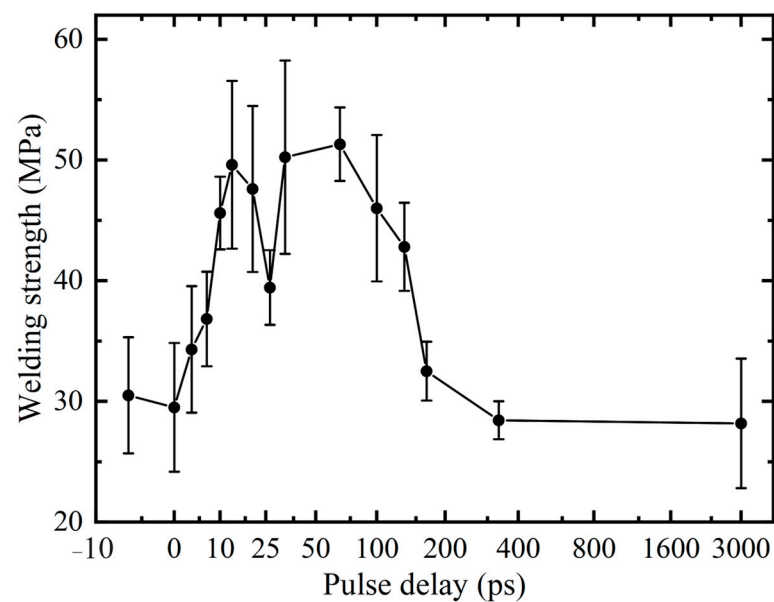
where c is the speed of light, taken as 3×10^8 m/s, Δx is the displacement of the one-dimensional moving platform, and τ is the delay time between the two pulses. The corresponding relationship between different displacements and pulse delays is shown in Table 1. It should be noted that when the displacement exceeds 500 mm, the range of the one-dimensional moving platform is exceeded. The optical platform ensures the accuracy within the range of 450 mm. Other experimental parameters are shown in Table 2. As shown in Figure 2, the relationship between welding strength and pulse delay in the case of the double pulse was observed. In order to minimize the error, at least five experiments were performed for each point, after which the average value was taken for graphing. For convenience of observation, the abscissa is displayed in logarithmic coordinates based on 10, where the point with a pulse delay less than 0 is a single pulse. It can be seen from Figure 2 that welding strength first increases and then decreases with the increase in pulse delay time. There are two strength peaks (at 13.3 ps and 66.7 ps, respectively) and one trough (at 26.7 ps) in the figure. When the pulse delay exceeds about 200 ps, the welding strength is equivalent to that of a single pulse. It can be predicted that when the pulse delay further increases beyond 3000 ps, the welding strength will not increase.

Table 1. The corresponding relationship between different platform displacements and pulse delays.

Platform Displacement (mm)	Pulse Delay (ps)	Platform Displacement (mm)	Pulse Delay (ps)
0	0	5	33.3
0.5	3.3	10	66.7
1	6.7	15	100
1.5	10	20	133.3
2	13.3	25	166.7
3	20	50	333.3
4	26.7	450	3000

Table 2. Other experimental parameters.

Power of Laser (mW)	Wavelength (nm)	Energy of Pulse (μ J)	Pulse Duration (fs)	Pulse Interval (μ s)	Scanning Interval (μ m)	Scanning Speed (μ m/s)	Repetition Rate (kHz)
3000	1060	4.878	216	1.626	50	1000	615

**Figure 2.** Welding strength under different pulse delays.

However, since only a single variable was considered, multi-level and multifactor experiments were carried out. The main welding parameters analyzed based on the above analysis and experimental experience are listed in Table 3.

Table 3. Experimental factors and their levels.

Pulse Delay (ps)	Average Power (mW)	Scanning Interval (μ m)	Scanning Speed (μ m/s)	Repetition Rate (kHz)
0	1500	10	500	75
13.3	2000	50	1000	307
26.7	2500	100	2000	615
66.7	3000	—	—	—
166.7	3500	—	—	—

A close orthogonal table was found according to the manual [39], and the required number of groups was obtained by combining the horizontal method, combination method, and juxtaposition method. After verification, the conditions for multivariate analysis of

variance were satisfied. Each set of experiments was repeated at least five times, and the average value was taken. As shown in Table 4, the maximum welding strength is obtained at 615 kHz. When the average power is low, varying the other parameters did not result in good welding strength. If the scanning interval was too large, the size of the effective connected part of the welded region would be reduced, thus reducing the welding reliability. Conversely, if the scanning interval was very narrow, the processing efficiency would be severely reduced. The laser focus would repeatedly scan the heat-affected area that had already been processed, causing an increase in the internal residual stress and negatively affecting the weld quality. These conclusions were drawn from the preliminary analysis of the table, which will be further analyzed in the following sections.

Table 4. Orthogonal test parameters and results.

Number	Pulse Delay (ps)	Average Power (mW)	Scanning Interval (μm)	Scanning Speed ($\mu\text{m/s}$)	Repetition Rate (kHz)	Welding Strength (MPa)
1	0	1500	10	500	75	0.5
2	0	2000	100	500	75	9.86
3	0	2500	10	1000	307	1.1
4	0	3000	50	1000	615	29.5
5	0	3500	50	2000	307	5.1
6	13.3	1500	100	2000	615	0.3
7	13.3	2000	50	1000	307	0.1
8	13.3	2500	10	500	75	1.2
9	13.3	3000	10	2000	615	46.7
10	13.3	3500	100	500	75	15.75
11	26.7	1500	50	1000	307	0
12	26.7	2000	10	1000	615	6.75
13	26.7	2500	100	2000	615	5.15
14	26.7	3000	100	500	307	7.175
15	26.7	3500	50	2000	75	0.5
16	66.7	1500	100	500	307	0
17	66.7	2000	10	2000	75	0
18	66.7	2500	50	500	75	0
19	66.7	3000	50	1000	307	16.75
20	66.7	3500	10	1000	615	57.15
21	166.7	1500	50	2000	615	3.4
22	166.7	2000	100	500	615	0.5
23	166.7	2500	10	2000	307	38.58
24	166.7	3000	100	1000	75	20.78
25	166.7	3500	10	500	75	0

Note: In the welding strength column, a value of 0 indicates a failed weld, while a value less than 1 indicates a successful weld that requires a tensile force less than the minimum value of the testing instrument or too small to be measured. A strength slightly greater than 1 indicates a low welding success rate and correspondingly low strength. When the strength value is much larger than 1, it indicates a good welding effect can be achieved under that parameter.

3.2. Influence of Fs Laser Parameters on the Heat-Affected Zone

The morphology of the heat-affected zone is closely related to welding strength; therefore, the effect of different pulse delays on the heat-affected zone was studied to analyze the intrinsic relationship between double-pulse femtosecond laser and welding strength.

Figure 3 shows the side view of the heat-affected zone when the pulse delay time value is 166.7 ps under double pulses, and the pulse number ranges from 100 to 107. The width of the heat-affected zone cannot be observed under pulse numbers 100 and 101, respectively. When the pulse number exceeds 104, the area of the heat-affected zone reaches saturation. Figure 4 shows the side view of the heat-affected zone for a range of pulse numbers from 100 to 107 for a single pulse. It can be observed that the width and height of the heat-affected zone gradually increase with an increase in the number of pulses, and the heat-affected zone shows a comet-like shape structure. It can be concluded that the

number of pulses has an effect on the heat-affected zone generated by both single-pulse and double-pulse welding. Based on these observations, eight groups of pulse numbers are selected, as shown in Table 5, which correspond to different radiation times.

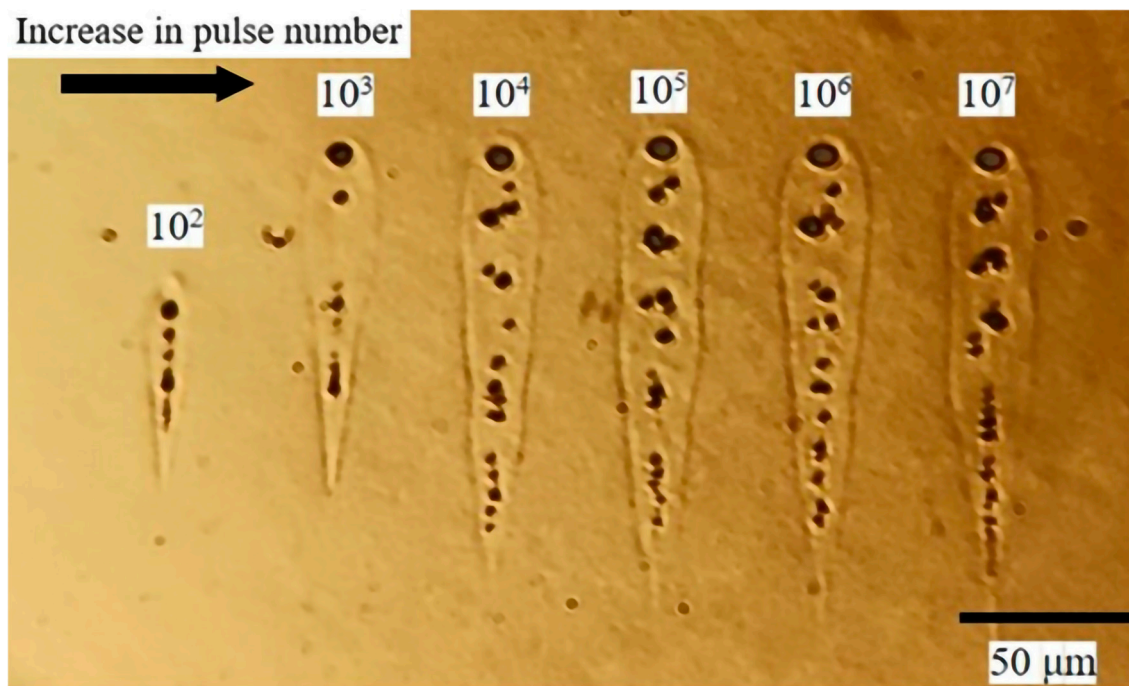


Figure 3. Side view of the heat-affected zone corresponding to different pulse numbers under double-pulse fs laser irradiation.

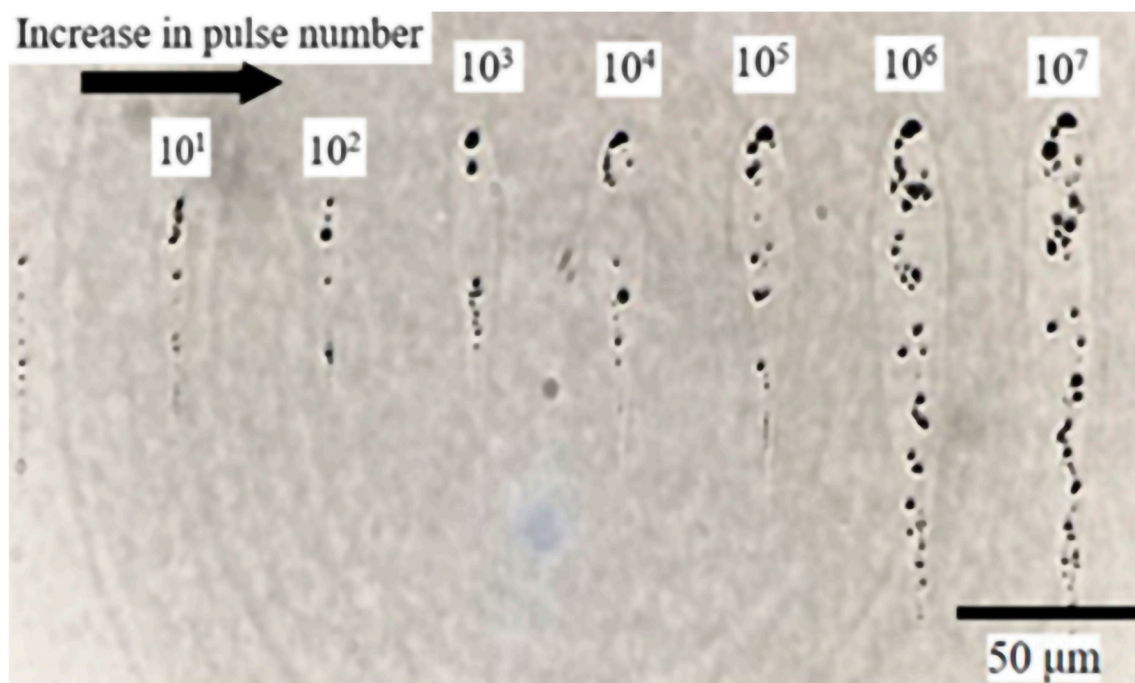


Figure 4. Side view of the heat-affected zone corresponding to different pulse numbers under repetitive single pulses fs laser irradiation.

Table 5. Number of pulses used in the experiment and corresponding irradiation time.

Number of pulses	30	70	100	400	700	1000	5000	10000
Irradiation time	48.8 μ s	113.8 μ s	162.6 μ s	650.4 μ s	1.1 ms	1.6 ms	8.1 ms	16.3 ms

Based on the pulse number of 8 groups, as shown in Table 5, the width of heat-affected zone, the pulse number, and the pulse delay curve were studied under different pulse delays. Figure 5a shows the variation curve between the width of the heat-affected zone and the number of pulses under different pulse delays. With an increase in the number of pulses, the width of the heat-affected zone gradually increases. However, the rate of increase is different for different pulse delays.

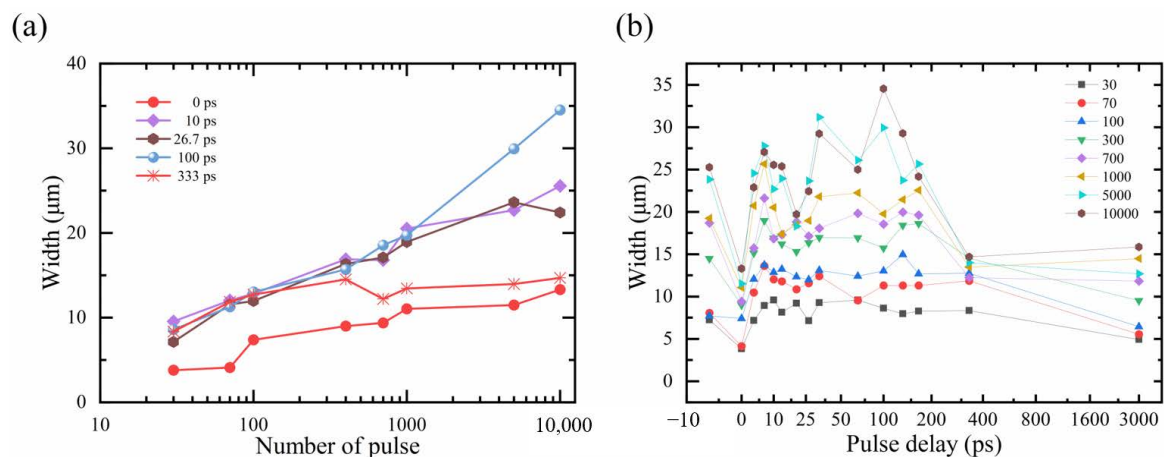


Figure 5. (a) The relationship between the heat-affected zone width and the pulse number. (b) The relationship between the heat-affected zone width and the pulse delay.

The growth rate of the width of the heat-affected zone is slow at 0 ps, maximum at 100 ps, and decreases relatively as the pulse delay time increases. The relationship between the width of the heat-affected zone and the pulse delay was studied under different pulse numbers, as shown in Figure 5b. When the number of pulses is small, the relationship between the width of the heat-affected zone and the pulse delay is not altered significantly but gradually becomes significant with an increase in the pulse number. When the pulse number reaches 104, the shift law of the curve is similar to the change law of welding strength (Figure 2) but not exactly the same. Therefore, the relationship between the area of the heat-affected zone and the pulse number and pulse delay was also investigated.

As shown in Figure 6a, the variation curve between the area of the heat-affected zone and the number of pulses under different pulse delays is presented. The area of the heat-affected zone increases with the pulse number, with a higher growth rate observed when the pulse number is small, and a lower growth rate when the pulse number is large. In the case of small pulse numbers, there is a slight difference in the area of the heat-affected zone formed by different pulse delays. Figure 6b shows the relationship between the area of the heat-affected zone and the pulse delay in different pulse numbers. When the pulse number is small, the curve is relatively smooth. When the pulse number reaches 10^4 , the heat-affected zone formed at the pulse delay of 0 ps and 26.7 ps is at different troughs, respectively. The welding strength increases as the pause delay increases from 33 ps to 100 ps, and the corresponding heat-affected zone area also increases. As the pulse delay continues to increase, the heat-affected zone decreases, and the welding strength also decreases.

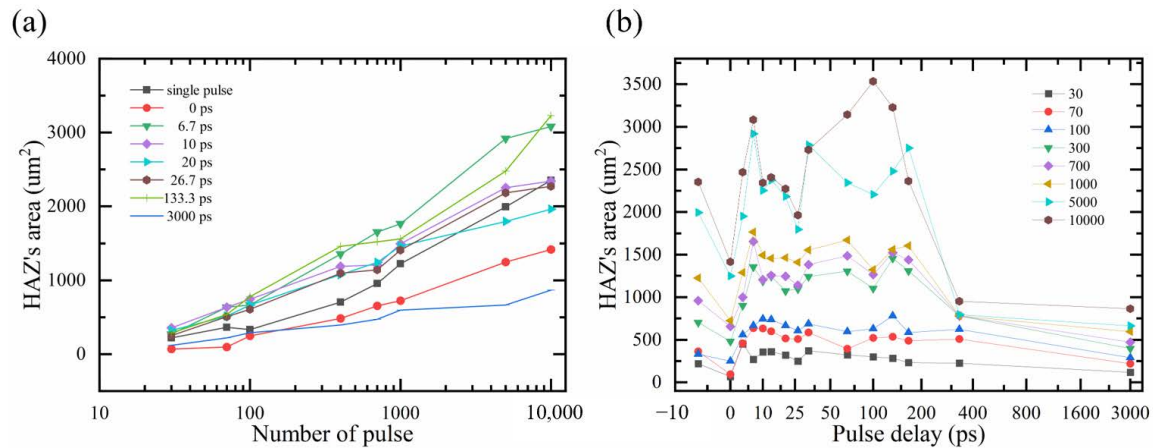


Figure 6. (a) The relationship between the area of the heat-affected zone and the pulse number. (b) The relationship between the area of the heat-affected zone and the pulse delay.

As shown in Figure 7, the heat-affected zone formed at a pulse delay value of 66.7 ps is larger than that formed at a pulse delay value of 3000 ps. Furthermore, from the vertical view, as shown in Figure 7b, a clear crack is observed, with the ablation region in the home view accounting for about 25%. On the left, it is only 15%. Therefore, it can be concluded that the welding strength corresponding to the 66.7 ps pulse delay is much larger than that corresponding to 3000 ps.

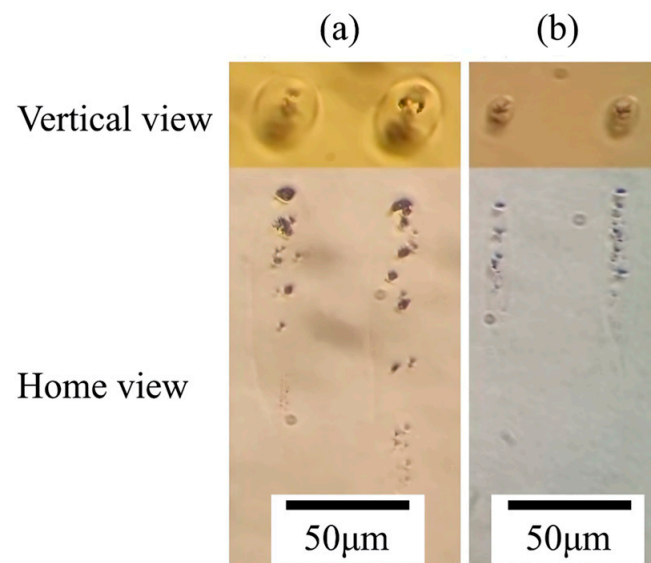


Figure 7. Vertical view and home view when (a) the pulse delay was 66.7 ps and the pulse number of 5000 and (b) the pulse delay of 3000 ps and the pulse number of 104, respectively.

In summary, when the number of pulses is sufficiently large, the relationship between the area of the heat-affected zone and the pulse delay follows a similar trend to that between the welding strength and the pulse delay. Therefore, Figure 6b can be used to predict the change in welding strength to some extent and find the optimal welding interval.

Other processing parameters were added to the original basis for the multi-factor study, and the three factors that had the greatest impact on the experimental results were chosen: pulse delay, average power, and repetition rate. The number of pulses was the same as above. Orthogonal experiments with three factors and three levels were designed, as shown in Table 6. Table 7 shows the size of the modified area obtained for different laser parameters in Table 6. The table shows that the largest modified area is number 6, and the smallest is number 4, which corresponds to the maximum and minimum laser power,

respectively. Figure 8 shows a side view of the glass modification area for different laser parameters corresponding to the numbers in the table, with a pulse number of 5000 in the figure. At a repetition rate of 615 kHz, a relatively pronounced thermal melting area is observed, and the modified area increases with the average power. When the repetition rate is low, the ablation area is more pronounced, and it increases with the average laser power. It can be concluded that the ratio of the ablation area to the thermal melting area can be controlled by controlling the repetition rate, and the size and shape of the modified area can be controlled by adjusting the repetition rate, pulse delay, and average power.

Table 6. Orthogonal experiment parameters.

Number	Pulse Delay (ps)	Average Power (mW)	Repetition Rate (kHz)
1	0	1500	75
2	0	2500	615
3	0	3500	307
4	66.7	1500	615
5	66.7	2500	307
6	66.7	3500	75
7	166.7	1500	307
8	166.7	2500	75
9	166.7	3500	615

Table 7. Size of modified zone area.

Number	1	2	3	4	5	6	7	8	9
Area (μm^2)	1522	706	1050	113	678	3542	359	2496	2550

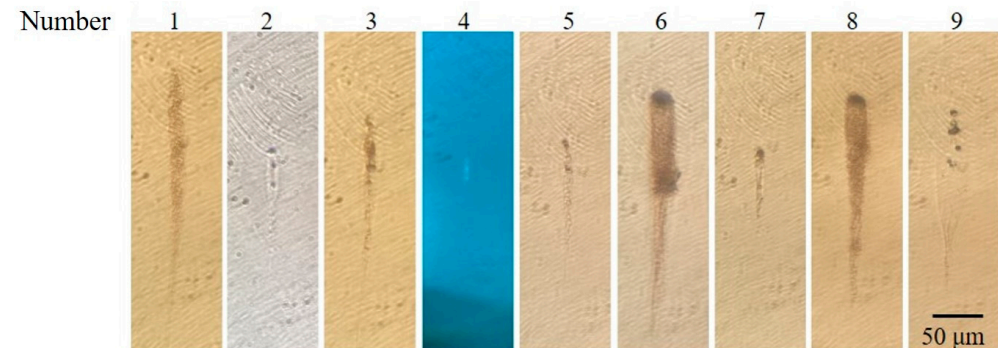


Figure 8. Side view of glass modification area under different laser parameters.

Tables 6 and 7 have been combined for a multivariate analysis of variance to analyze the relationship among repetition rate, average power, pulse delay, and modified area. The results of the multivariate analysis of variance are presented in Table 8. The R^2 value of 0.9786 suggests that these three factors can account for 97.86% of the variation in the modified area. The average power is significant ($F = 19.294$, $p = 0.049 < 0.05$) and has a differential relationship with the area. Similarly, the repetition rate is also significant ($F = 23.306$, $p = 0.041 < 0.05$), and it has a differential relationship with area. However, the pulse delay is not significant ($F = 3.217$, $p = 0.237 > 0.05$) and does not have a differential relationship with area. Therefore, it can be concluded that the effect of the former two factors on the modified area is larger than that of the pulse delay.

Table 8. Results of multivariate analysis of variance(The three factors).

	Sum of Squares	Df	Mean Square	F	p
Intercept	18,824,028.444	1	18,824,028.444	160.627	0.006 **
Repetition Rate	5,462,414.889	2	2,731,207.444	23.306	0.041 *
Average power	4,522,171.556	2	2,261,085.778	19.294	0.049 *
Pulse delay	754,037.556	2	377,018.778	3.217	0.237
Residual	234,381.556	2	117,190.778	—	—

Note: $R^2 = 0.9786$, * $p < 0.05$, ** $p < 0.01$.

3.3. Significance Analysis of Fs Laser Parameters on Welding Strength

After analyzing the data in Table 4, the relationship between fs laser parameters and welding strength can be preliminarily established. To determine the effect of these factors on welding strength, the data were analyzed quantitatively using SPSS data analysis software. Table 9 shows that five influencing factors were analyzed, and based on an R^2 value of 0.938, it can be inferred that these factors can explain 93.8% of the variation in the modified area.

Table 9. Results of multivariate analysis of variance(The five factors).

	Sum of Squares	Df	Mean Square	F	p
Intercept	2908.821	1	2908.821	13.003	0.005 **
Pulse delay	433.666	4	108.417	0.485	0.747
Average power	1765.244	4	441.311	1.973	0.175
Scanning interval	542.791	2	271.396	1.213	0.338
Scanning speed	148.720	2	74.360	0.332	0.725
Repetition rate	526.056	2	263.028	1.176	0.348
Residual	2237.032	10	223.703	—	—

Note: $R^2 = 0.938$, ** $p < 0.01$.

In SPSS data analysis software, the three-factor variance was selected from the Advanced Method TAB for the data in Table 8. The pulse delay, average power, and repetition rate were set as X variables, and the intensity was set as the Y variable. The analysis results in Table 10 show that the pulse delay, average power, and repetition rate have a differential relationship with welding strength. Additionally, a three-factor analysis of variance was performed on scanning interval, scanning speed, and pulse delay to determine their influence on welding strength. Table 11 indicates that the scan spacing and scanning speed do not have a differential relationship with intensity, while the pulse delay does.

Table 10. Results of three-factor analysis of variance for pulse delay, average power, and repetition rate.

Differences between the Source	Sum of Squares	Df	Mean Square	F	p
Intercept	3239.786	1	3239.786	14.783	0.002 **
Pulse delay	545.779	4	136.445	0.623	0.049
Average power	2220.383	4	555.096	2.533	0.007
Repetition rate	903.582	2	451.791	2.061	0.04
Residuals	3068.268	14	219.162	—	—

Note: $R^2 = 0.828$, ** $p < 0.01$.

Based on the above analysis, the order of the influencing factors on welding strength, from most significant to least, is average power > repetition rate > pulse delay > scanning interval > scanning speed. In multiple experiments, when the average power is 3500 mW, the repetition rate is 615 kHz, the pulse delay is 66.7 ps, the scanning interval is 10 μm , and the scanning speed is 1000 $\mu\text{m/s}$, the optimal welding strength is 57.15 MPa, which is about 50% higher than that of the single pulse welding strength shown in Figure 2. It is important to note that higher single pulse energy can cause severe ablation on silica glass. When

it exceeds hundreds of microjoules, SiO₂ will be directly eroded in the form of powder, forming a micro-shock wave at the focus, which significantly increases the probability of glass cracking. Therefore, femtosecond lasers with high pulse energy at higher single pulse energy are not suitable for silica glass welding.

Table 11. Results of three-factor analysis of variance for scan spacing, scan speed, and pulse delay.

Differences between the Source	Sum of Squares	Df	Mean Square	F	p
Intercept	2923.835	1	2923.835	10.762	0.005 **
Scanning interval	569.667	2	284.833	1.048	0.181
Scanning speed	1034.944	2	517.472	1.905	0.373
Pulse delay	438.232	4	109.558	0.403	0.05
Residuals	4347.015	16	271.688	—	—

Note: $R^2 = 0.297$, ** $p < 0.01$.

3.4. Analysis of Fs Laser Parameters on Welding Strength through Fracture Morphology of the Welding Interface

The fracture morphology of the welding interface was observed to analyze the characteristics under different parameters. Figure 9 shows the welding fracture patterns corresponding to the numbers in Table 4, which reveals the laser power range of 1500 mW to 3500 mW with a repetition rate of 75 kHz. The higher single pulse energy was obtained with higher laser power, resulting in a stronger ablation effect on glass.

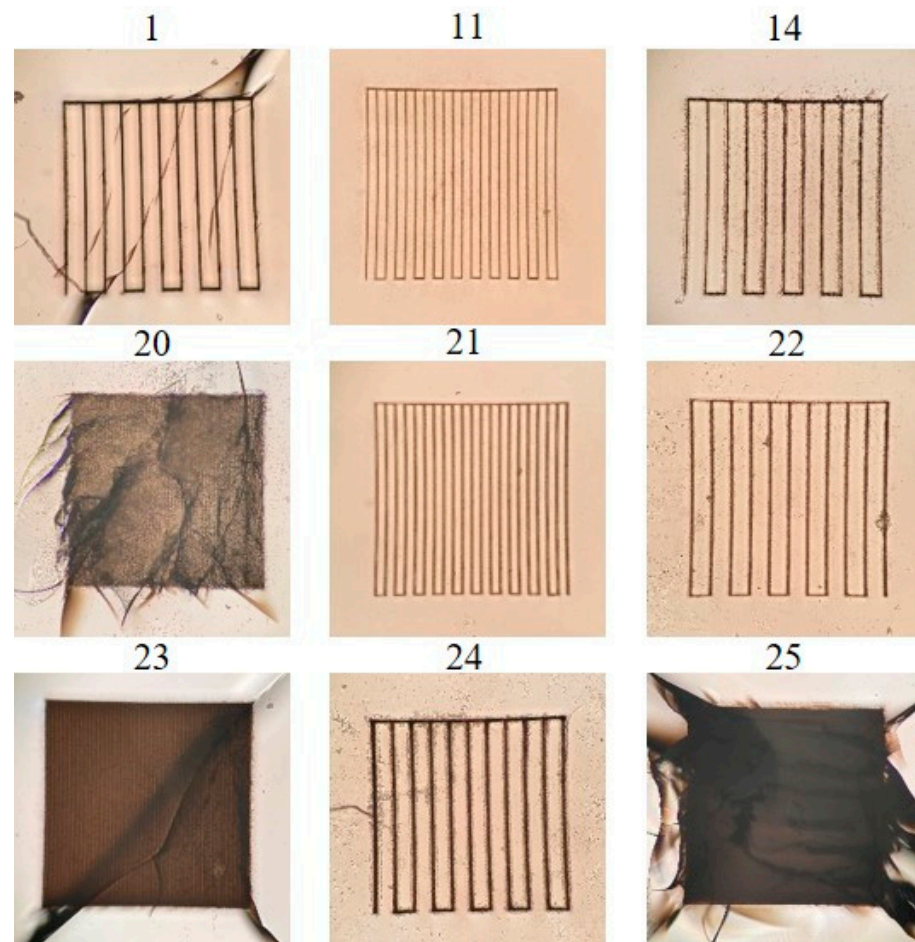


Figure 9. The fracture morphology of the welding interface under different processing parameters (the numbers in the figure correspond to those in Table 4).

The scanning interval of No. 24 is larger than that of NO. 25, with other parameters being the same. Large cracks were observed in NO. 25 due to the strong ablation effect and large internal stress, resulting in a failed welding. A proper interval benefits to reduce internal stress and obtain high welding strength.

Although reducing the average power can reduce the ablation effect, it is still difficult to achieve glass welding at low repetition rates. When the repetition rate increases to 307 kHz, the heat accumulation effect of multiple pulses is enhanced with a simultaneous reduced ablation effect, resulting in higher welding strength than that obtained at a lower repetition rate. But the welding strength is different under different average power. The laser power and pulse energy of NO. 11 is low, producing not enough molten pools for successful welding. As the power increases and the scanning interval decreases, the produced molten pool is able to fill the gap between the pieces for good welding strength, as shown in NO.14. However, for large pulse energy and small scanning intervals, as used in NO. 23, cracks were generated due to internal residual stress.

When the repetition rate continues to increase to 615 kHz, its multiple pulse heat accumulation effect is significant. As a result, the maximum welding strength is obtained for the No. 20, it produces a molten pool that adequately fills the gaps between the sample. The shrinkage effect produced after cooling pulls the distance between the samples to $\lambda/4$, while the cracks in the figure are produced after conducting the shear test. The area to be welded is fractured as a whole, also indicating that the molten pool it produces adequately fills the gap between the samples. No. 21 and No. 22 show the shape formed by further reducing the pulse energy and increasing the scanning interval, which makes it difficult to weld effectively because the molten pool produced by welding is not sufficient to fill the gap. A high welding strength can be obtained by proper interval and average power. When the average power is 3500 mW, the repetition rate is 615 kHz, the pulse delay is 66.7 ps, the scanning interval is 10 μm , and the scanning speed is 1000 $\mu\text{m/s}$, high welding strength can be obtained.

3.5. Temperature Resistance

The temperature resistance of the silica glass has been tested, as it may be subjected to high temperatures during use. Optimal parameters were selected for the test, including an average laser power of 3500 mW, a repetition rate of 615 kHz, a pulse delay of 66.7 ps, a scanning interval of 10 μm , and a scanning speed of 1000 $\mu\text{m/s}$. The samples were bonded with Fix-All adhesive (Soudal, Turnhout, Belgium) and left for 20 min before being compared to the welded samples. As shown in Figure 10a, the two sets of samples were placed on a heating table and heated according to the method shown in Figure 11. The temperature was increased at room temperature and recorded every minute, reaching 300 °C at the 12th minute, holding for 20 min, and then cooling every 10 min. The temperature was lowered to 39 °C at around the 62nd minute, and three temperature changes were carried out for each group of samples. Three sets of experiments were carried out in total. The adhesive-bonded samples failed to maintain their connection during the first temperature rise and could be easily separated by tweezers, while the welded samples maintained good connection performance throughout the entire process. As shown in Figure 10b, the welded samples on the left maintained good connection performance, while the adhesive-bonded samples on the right could be easily separated. Therefore, it can be concluded that silica glass welded by femtosecond laser has excellent high-temperature resistance and thermal shock resistance compared to silica glass bonded with adhesive.

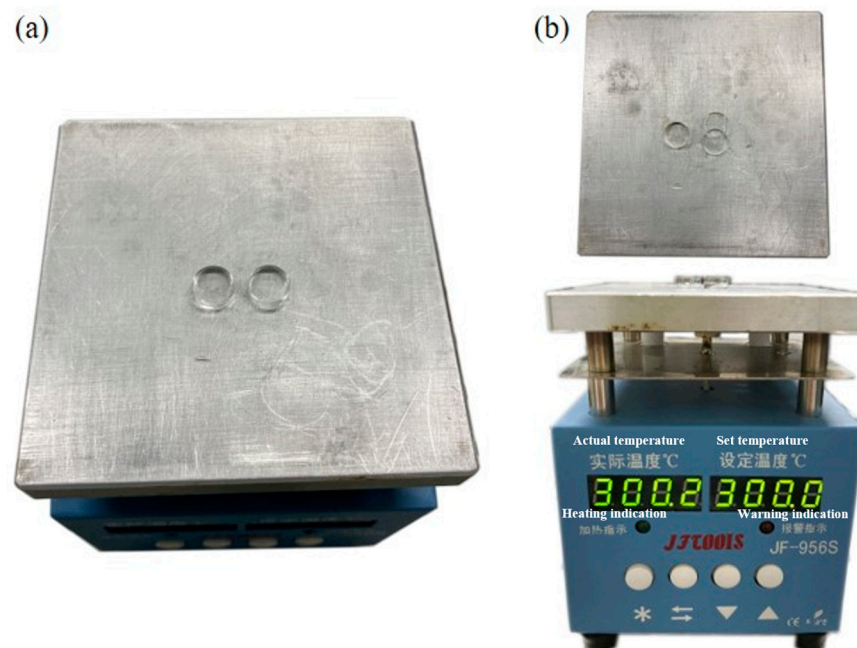


Figure 10. (a) Two samples in heating (the left is the welded sample, and the right is the adhesive connection sample). (b) The thermal insulation state of the sample.

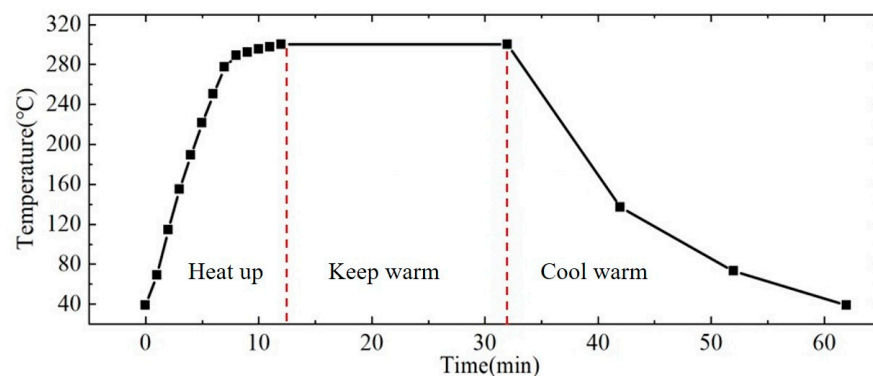


Figure 11. Process of temperature change.

4. Conclusions

A method for welding silica glass with a double-pulse femtosecond laser is presented. This method increases the heat-affected zone more efficiently and achieves higher welding strength than previous laser welding methods. By optimizing the parameters, a welding strength of 57.15 MPa is obtained when the average power is 3500 mW, the repetition rate is 615 kHz, the pulse delay is 66.7 ps, the scanning interval is 10 μm , and the scanning speed is 1000 $\mu\text{m/s}$. The efficiency of this method and the quality of the resulting welds underscore its potential applications in aerospace, microelectronic packaging, and microfluidics. The research also emphasizes the significance of pulse delay in influencing the heat-affected zone and, consequently, the welding strength, with optimal performance observed at a delay of 66.7 ps. Temperature resistance tests further confirmed the robustness of the welded silica glass, which maintained its integrity under extreme thermal conditions. Femtosecond laser welding demonstrates superior performance compared to other methods, including nanosecond lasers, by minimizing heat-affected zones and reducing thermal distortion. This leads to faster, more efficient, and precise welding of transparent materials, which is crucial for high-throughput applications that require minimal material alteration. Future research should focus on optimizing the welding process for various types of glass and transparent materials, automating systems for industrial applications, and assessing the long-term

stability of these welds under different conditions, particularly for critical applications in aerospace and medical devices.

Author Contributions: Conceptualization, Z.G. and J.H.; methodology, X.J.; software, Z.Y.; validation, C.L., S.Z.; investigation, C.W.; resources, J.D.; writing—original draft preparation, Z.G.; writing—review and editing, J.H. and Z.Y.; supervision, X.J.; project administration, C.W. All authors have read and agreed to the published version of the manuscript.

Funding: This research was funded by the Natural Science Foundation of China (Grant No. 52105498), the State Key Laboratory of Precision Manufacturing for Extreme Service Performance (Grant No. ZZYJKT2023-08), the National Natural Science Foundation of China Joint Fund for Regional Innovation Development (Hunan Province, U22A20200), and the National Key R&D Program of China (Grant No. 2023YFB4605500).

Institutional Review Board Statement: Not applicable.

Informed Consent Statement: Not applicable.

Data Availability Statement: No new data were created or analyzed in this study. Data sharing does not apply to this study.

Conflicts of Interest: The authors declare no competing financial interests.

References

- Weller, B.; Schadow, T. Research and development in the structural use of glass. *Stahlbau* **2007**, *76*, 162–166. [\[CrossRef\]](#)
- Kawakita, M.; Iwasawa, S.; Lopez-Gulliver, R.; Inoue, N. Glasses-free large-screen three-dimensional display and super multiview camera for highly realistic communication. *Opt. Eng.* **2018**, *57*, 061610. [\[CrossRef\]](#)
- Goyal, R.; Vishwakarma, D.K. Design of a graphene-based patch antenna on glass substrate for high-speed terahertz communications. *Microw. Opt. Technol. Lett.* **2018**, *60*, 1594–1600. [\[CrossRef\]](#)
- Chang, Y.H.; Chen, J.C.; Chung, W.; Li, W.Y.; Shih, P.T.B.; Ng’oma, A.; Yang, C.; Huang, M.-C.; Lin, H.-Y.; Wang, C.-H. A novel fabrication process and measurement results of a 28 GHz glass antenna with single TGV for 5G communication applications. In Proceedings of the 2019 14th International Microsystems, Packaging, Assembly and Circuits Technology Conference (IMPACT), Taipei, Taiwan, 23–25 October 2019; pp. 112–115.
- Kang, D.S.; Lee, E.M.; Dal-Young, K. A Questionnaire Study on Introduction of Military Optician and Eye-glasses Supply System to the Korean Armed Forces. *Korean J. Vis. Sci.* **2011**, *13*, 1–9.
- Byun, G.; Seo, C.; Jang, B.-J.; Choo, H. Design of a double-faced glass-integrated antenna for military aircraft FM radio communication. In Proceedings of the 2011 IEEE International Symposium on Antennas and Propagation (APSURSI), Spokane, WA, USA, 3–8 July 2011; pp. 1784–1787.
- Montechiaro, L.; Kaefer, I.L.; Quadros, F.C.; Cechin, S. Feeding habits and reproductive biology of the glass lizard *Ophiodon cf. striatus* from subtropical Brazil. *North-West. J. Zool.* **2011**, *7*, 63–71.
- Carey, L.A. Through a Glass Darkly: Advances in Understanding Breast Cancer Biology, 2000–2010. *Clin. Breast Cancer* **2010**, *10*, 188–195. [\[CrossRef\]](#)
- Milanese, D.; Pugliese, D.; Boetti, N.G.; Ceci-Ginistrelli, E.; Janner, D.; Sglavo, V.; Vitale-Brovarone, C.; Lousteau, J. Phosphate glass fibers for optical amplifiers and biomedical applications. In Proceedings of the Optical Fiber Communication Conference, Los Angeles, CA, USA, 19–27 March 2017; Optical Society of America: Washington, DC, USA, 2017; p. M2F.
- Pan, Y.J.; Yang, R.J. A glass microfluidic chip adhesive bonding method at room temperature. *J. Micromech. Microeng.* **2006**, *16*, 2666–2672. [\[CrossRef\]](#)
- de Pablos-Martin, A.; Tismer, S.; Naumann, F.; Krause, M.; Lorenz, M.; Grundmann, M.; Hoeche, T. Evaluation of the bond quality of laser-joined sapphire wafers using a fresnoite-glass sealant. *Microsyst. Technol.* **2016**, *22*, 207–214. [\[CrossRef\]](#)
- Aran, K.; Sasso, L.A.; Kamdar, N.; Zahn, J.D. Irreversible, direct bonding of nanoporous polymer membranes to PDMS or glass microdevices. *Lab A Chip* **2010**, *10*, 548–552. [\[CrossRef\]](#)
- Katayama, S. *Handbook of Laser Welding Technologies*; Elsevier: Amsterdam, The Netherlands, 2013.
- Elrefaey, A.; Janczak-Rusch, J.; Koebel, M. Direct glass-to-metal joining by simultaneous anodic bonding and soldering with activated liquid tin solder. *J. Mech. Work. Technol.* **2014**, *214*, 2716–2722. [\[CrossRef\]](#)
- Pohl, L.; von Witzendorff, P.; Chatzizyrlis, E.; Suttman, O.; Overmeyer, L. CO₂ laser welding of glass: Numerical simulation and experimental study. *Int. J. Adv. Manuf. Technol.* **2017**, *90*, 397–403. [\[CrossRef\]](#)
- Li, Z.; Mo, H.; Tian, J.; Li, J.; Xia, S.; Jia, X.; Zhou, L.; Lu, Y. Compressive Properties and Fracture Behaviours of Ti/Al Interpenetrating Phase Composites with Additive-Manufactured Triply Periodic Minimal Surface Porous Structures. *Met. Mater. Int.* **2024**. [\[CrossRef\]](#)
- Li, Z.; Lin, J.; Jia, X.; Li, X.; Li, K.; Wang, C.; Sun, K.; Ma, Z.; Duan, J. High Efficiency Femtosecond Laser Ablation of Alumina Ceramics under the Filament Induced Plasma Shock Wave. *Ceram. Int.* **2024**. [\[CrossRef\]](#)

18. Li, Z.; Lin, J.; Wang, C.; Li, K.; Jia, X.; Wang, C.; Duan, J.A. Damage performance of alumina ceramic by femtosecond laser induced air filamentation. *Opt. Laser Technol.* **2025**, *181*, 111781. [\[CrossRef\]](#)
19. Taylor, I.J.A. *Use of Infrared Dyes for Transmission Laser Welding of Plastics*; SPE: Richardson, TX, USA, 2000; pp. 1166–1170.
20. Jia, X.; Chen, Y.; Liu, L.; Wang, C.; Duan, J.A. Combined pulse laser: Reliable tool for high-quality, high-efficiency material processing. *Opt. Laser Technol.* **2022**, *153*, 108209. [\[CrossRef\]](#)
21. Wang, J.; Fang, F.; An, H.; Wu, S.; Qi, H.; Cai, Y.; Guo, G. Laser Machining Fundamentals: Micro, Nano, Atomic and Close-to-Atomic Scales. *Int. J. Extrem. Manuf.* **2023**, *5*, 012005. [\[CrossRef\]](#)
22. Matsumoto, F.; Yamada, M.; Tsuta, M.; Nakamura, S.; Ando, N.; Soma, N. Review of the Structure and Performance of Through-Holed Anodes and Cathodes Prepared with a Picosecond Pulsed Laser for Lithium-Ion Batteries. *Int. J. Extrem. Manuf.* **2023**, *5*, 012001. [\[CrossRef\]](#)
23. Balage, P.; Lopez, J.; Bonamis, G.; Hönninger, C.; Manek-Hönninger, I. Crack-Free High-Aspect Ratio Holes in Glasses by Top-down Percussion Drilling with Infrared Femtosecond Laser GHz-Bursts. *Int. J. Extrem. Manuf.* **2023**, *5*, 015002. [\[CrossRef\]](#)
24. Jia, X.; Chen, Y.; Liu, L.; Wang, C.; Duan, J. Advances in Laser Drilling of Structural Ceramics. *Nanomaterials* **2022**, *12*, 230. [\[CrossRef\]](#)
25. Jia, X.; Li, Z.; Wang, C.; Li, K.; Zhang, L. Study of the dynamics of material removal processes in combined pulse laser drilling of alumina ceramic. *Opt. Laser Technol.* **2023**, *160*, 109053. [\[CrossRef\]](#)
26. Xiao, H.; Zhang, W.; Zhou, Y.; Liu, M.; Zhou, G. A Numerical Simulation and Experimental Study on the Ultrafast Double-Laser Precision Cutting of Sapphire Materials. *Crystals* **2022**, *12*, 867. [\[CrossRef\]](#)
27. Jia, X.; Li, K.; Li, Z.; Wang, C.; Chen, J.; Cui, S. Multi-scan picosecond laser welding of non-optical contact soda lime glass. *Opt. Laser Technol.* **2023**, *161*, 109164. [\[CrossRef\]](#)
28. Tamaki, T.; Watanabe, W.; Itoh, K. Laser micro-welding of transparent materials by a localized heat accumulation effect using a femtosecond fiber laser at 1558 nm. *Opt. Express* **2006**, *14*, 10460–10468. [\[CrossRef\]](#) [\[PubMed\]](#)
29. Sugioka, K. Progress in ultrafast laser processing and future prospects. *Nanophotonics* **2017**, *6*, 393–413. [\[CrossRef\]](#)
30. Tamaki, T.; Watanabe, W.; Nishii, J.; Itoh, K. Welding of transparent materials using femtosecond laser pulses. *Jpn. J. Appl. Phys. Part 2-Lett. Express Lett.* **2005**, *44*, L687–L689. [\[CrossRef\]](#)
31. Watanabe, W.; Onda, S.; Tamaki, T.; Itoh, K.; Nishii, J. Space-selective laser joining of dissimilar transparent materials using femtosecond laser pulses. *Appl. Phys. Lett.* **2006**, *89*, 021106. [\[CrossRef\]](#)
32. Watanabe, W.; Onda, S.; Tamaki, T.; Itoh, K. Direct joining of glass substrates by 1 kHz femtosecond laser pulses. *Appl. Phys. B Laser Opt.* **2007**, *87*, 85–89. [\[CrossRef\]](#)
33. Richter, S.; Döring, S.; Tünnermann, A.; Nolte, S. Bonding of glass with femtosecond laser pulses at high repetition rates. *Appl. Phys. A* **2011**, *103*, 257–261. [\[CrossRef\]](#)
34. Hélie, D.; Bégin, M.; Lacroix, F.; Vallée, R. Reinforced direct bonding of optical materials by femtosecond laser welding. *Appl. Opt.* **2012**, *51*, 2098–2106. [\[CrossRef\]](#)
35. Kim, S.; Kim, J.; Joung, Y.-H.; Choi, J.; Koo, C. Bonding Strength of a Glass Microfluidic Device Fabricated by Femtosecond Laser Micromachining and Direct Welding. *Micromachines* **2018**, *9*, 639. [\[CrossRef\]](#)
36. Miao, Y.; Ting, H.; Rongshi, X. Long focal length green femtosecond laser welding of glass. *Chin. J. Lasers* **2020**, *47*, 0902005. [\[CrossRef\]](#)
37. Zhang, S.; Kong, M.; Miao, H.; Memon, S.; Zhang, Y.; Liu, S. Transient temperature and stress fields on bonding small glass pieces to solder glass by laser welding: Numerical modelling and experimental validation. *Sol. Energy* **2020**, *209*, 350–362. [\[CrossRef\]](#)
38. Sugioka, K.; Iida, M.; Takai, H.; Micorikawa, K. Efficient microwelding of glass substrates by ultrafast laser irradiation using a double-pulse train. *Opt. Lett.* **2011**, *36*, 2734–2736. [\[CrossRef\]](#) [\[PubMed\]](#)
39. SPSSAU. The SPSSAU Project (Version 20.0). [Online Application Software]. 2020. Available online: <https://www.spssau.com> (accessed on 17 April 2024).

Disclaimer/Publisher’s Note: The statements, opinions and data contained in all publications are solely those of the individual author(s) and contributor(s) and not of MDPI and/or the editor(s). MDPI and/or the editor(s) disclaim responsibility for any injury to people or property resulting from any ideas, methods, instructions or products referred to in the content.